Reaction of O2 +(X 2Π g) with H2, D2, and HD: Guided ion beam studies, MO correlations, and statistical theory calculations

M. E. Weber, N. F. Dalleska, B. L. Tjelta, E. R. Fisher, and P. B. Armentrout

Citation: The Journal of Chemical Physics **98**, 7855 (1993); doi: 10.1063/1.464593
View online: http://dx.doi.org/10.1063/1.464593
View Table of Contents: http://scitation.aip.org/content/aip/journal/jcp/98/10?ver=pdfcov
Published by the AIP Publishing

Reaction of $O_2^+(X\,^2\Pi_g)$ with H_2, D_2, and HD: Guided ion beam studies, MO correlations, and statistical theory calculations

M. E. Weber,[a] N. F. Dalleska, B. L. Tjelta, E. R. Fisher, and P. B. Armentrout
Department of Chemistry, University of Utah, Salt Lake City, Utah 84112

(Received 8 January 1993; accepted 8 February 1993)

Absolute cross sections are measured for the reactions of $O_2^+(X\,^2\Pi_g)$ with H_2, D_2, and HD from thermal energies to over 4 eV. The $OH^+ + OH$, $HO_2^+ + H$, $O^+ + H_2O$, and $H_2O^+ + O$ product channels (and the corresponding isotopic analogs) are observed, although $H_2^+ + O_2$ is not. While the first three products appear at their thermodynamic thresholds, formation of $H_2O^+ + O$, the least endothermic channel, exhibits a barrier to reaction. In the HD system, the DO_2^+ product ion is strongly favored over the HO_2^+ product. Results for internally excited O_2^+ reactants, probably the $a\,^4\Pi_u$ state, are also presented. Analysis of the excitation functions, molecular orbital arguments, and statistical kinetic theories are used to understand the mechanisms and dynamics of this reaction. It is shown that the inefficiency of the O^+ product channel is due to spin and symmetry constraints. The other three product channels proceed through a long-lived intermediate, but formation of this intermediate from reactants requires surmounting a barrier measured to be 1.1 ± 0.1 eV. The intramolecular isotope effects are shown to be due to statistical and dynamic effects.

I. INTRODUCTION

The reactions of O_2^+ with molecular hydrogen have been of significant interest over the past three decades, and various aspects of these reactions have been investigated. Several studies have examined the thermal reactivity of O_2^+ and these show that the $X\,^2\Pi_g$ ground state is unreactive with H_2 while the metastable $a\,^4\Pi_u$ state reacts efficiently.[1–4] State-specific *relative* cross sections have been measured for O_2^+ consisting of the $v=19$ and 20 vibrational levels of $O_2^+(X\,^2\Pi_g)$ and for the $v=0$–7 levels of metastable $O_2^+(a\,^4\Pi_u)$.[5] However, these studies included only reactions with H_2 and HD to produce H_2^+, HO_2^+, and DO_2^+ at only one kinetic energy, 0.25 eV in the H_2 system and 0.4 eV in the HD system.

More detailed studies of the reactions of ground state O_2^+ with H_2 come from the work of Mahan and coworkers.[6] In order to probe the dynamics of the title reactions, they measured differential cross sections for the product ions. They established that OH^+ and HO_2^+ are produced through a long-lived intermediate at low interaction energies, but above ~ 5 eV, these reactions proceed via a direct mechanism. The observed isotope effects in the reaction with HD corroborated these conclusions, as did studies by Ding and Henglein.[7] Mahan's studies also demonstrated that H_2O^+ formation proceeds through a long-lived intermediate, even at 6 eV. However, the intensity of this product was less than those of OH^+ and HO_2^+, even though formation of H_2O^+ is the least endothermic reaction channel. This suggested that H_2O^+ formation is restricted by either an energy barrier or dynamic constraints. Based on molecular orbital correlation arguments[8] and appearance energy measurements of Foner and Hudson,[9] Mahan and co-workers concluded that there is a 2.5 ± 0.5 eV barrier in the entrance channel of the $O_2^+ + H_2$ reaction.[6]

In the present work, we use guided ion-beam mass spectrometry to examine the reactions of vibrationally cold ground-state $O_2^+(X\,^2\Pi_g)$ with H_2, D_2, and HD. We measure the energy dependence of the *absolute* integral cross sections from thermal energy to over 4 eV in the center-of-mass frame of reference. Results for internally excited O_2^+ ions reacting with D_2 and HD are also presented. Although the assignment of the state of these ions is equivocal, the results are consistent with the dominant state being the $a\,^4\Pi_u$ electronic state. The experimental excitation functions are analyzed in detail and interpreted by extending the molecular orbital correlation arguments of Mahan[8] and by comparison with results of statistical phase space theory (PST) and with a theory that considers a tight transition state.

Previously in our laboratory, we have applied PST to several atom–diatom ion–molecule reactions by adapting computer programs from Bowers, Chesnavich, and others.[10] In such systems, the PST calculations modeled experimental reaction cross sections extremely well, and provided information on the thermochemistry,[11–13] reactive potential surfaces,[14] and angular momentum effects.[15] However, PST calculations involving larger systems, such as the diatom–diatom title reactions, are more complicated. First, more product channels are available, and determination of the reactive potential surfaces is more complex. Second, the increased degrees of freedom require knowledge of a greater number of molecular parameters for each channel. Finally, rigorous conservation of angular momentum is complicated by the increase in rotational degrees of freedom, so that additional assumptions are required.[16]

Nevertheless, PST calculations are readily applied to the reactions of O_2^+ with hydrogen, because all of the molecular parameters necessary for the calculations are either

[a]Present address: NASA, Johnson Space Center, Houston, TX 77058.

 0021-9606/93/107855-13$06.00

TABLE I. Heats of Formation at 0 K (kcal/mol).[a]

Neutral	$\Delta_f H^0$	Ion	$\Delta_f H^0$
H	51.634±0.001	H_2^+	355.726±0.001
D	52.535±0.001	D_2^+	356.665±0.003
HD	0.079±0.002	HD^+	356.238±0.005
O	58.984±0.024	O^+	373.024±0.024
OH	9.3 ±0.3	OH^+	309.0 ±0.2[b]
OD	8.6 ±0.3	OD^+	308.7 ±0.2[c]
H_2O	−57.10 ±0.01	H_2O^+	233.7 ±0.2[b]
D_2O	−58.86 ±0.02	D_2O^+	232.5 ±0.2[b]
HDO	−57.94 ±0.02	HDO^+	233.1 ±0.2[d]
HO_2	4.5 ±1.2[e]	HO_2^+	266.2 ±1.2[f]
		DO_2^+	265.1 ±2.0[c]
		O_2^+	278.37 ±0.12

[a]Taken from the JANAF tables (Ref. 21) unless otherwise noted.
[b]Reference 24.
[c]Calculated by using molecular information given in Table IV.
[d]Calculated from IE(HDO)=12.62 eV taken from Ref. 40.
[e]E. R. Fisher and P. B. Armentrout, J. Phys. Chem. **94** 4396 (1990). Conversion to 0 K given by C. J. Howard, J. Am. Chem. Soc. **102**, 6937 (1980).
[f]Calculated by using IE(HO_2)=11.35±0.01 eV from Ref. 39.

known or can be accurately estimated. The application of PST to these reactions is appropriate because the previous experiments suggest that the reactions proceed through long-lived, strongly coupled intermediates at low kinetic energies,[6,7] a necessary assumption for PST. A difficulty arises, however, because there is evidence for a tight transition state in the entrance channel,[8] a feature that is not assimilated in PST calculations. To overcome this, we have also utilized a theory for translationally driven reactions as outlined by Chesnavich and Bowers,[17] who adapted a treatment of Marcus,[18] who in turn expanded and elaborated an idea of Safron *et al.*[19]

Thermochemistry

For reaction of $O_2^+(X\,^2\Pi_g)$ with H_2, there are six energetically accessible product channels in the energy range studied here. All are endothermic and are given in reactions (1a)–(5a), along with the 0 K literature endothermicities calculated by using the heats of formation given in Table I:

$$O_2^+ + H_2 \rightarrow OH^+ + OH, \quad \Delta H = 1.73 \pm 0.02 \text{ eV} \quad (1a)$$
$$\rightarrow HO_2^+ + H, \quad \Delta H = 1.71 \pm 0.05 \text{ eV} \quad (2a)$$
$$\rightarrow H_2O^+ + O, \quad \Delta H = 0.62 \pm 0.01 \text{ eV} \quad (3a)$$
$$\rightarrow O^+ + H_2O, \quad \Delta H = 1.63 \pm 0.01 \text{ eV} \quad (4a)$$
$$\rightarrow H_2^+ + O_2, \quad \Delta H = 3.35 \pm 0.01 \text{ eV}. \quad (5a)$$

Likewise, the accessible product channels and heats of reaction for the D_2 system are given in reactions (1b)–(5b):

$$O_2^+ + D_2 \rightarrow OD^+ + OD, \quad \Delta H = 1.69 \pm 0.02 \text{ eV} \quad (1b)$$
$$\rightarrow DO_2^+ + D, \quad \Delta H = 1.70 \pm 0.09 \text{ eV} \quad (2b)$$
$$\rightarrow D_2O^+ + O, \quad \Delta H = 0.57 \pm 0.01 \text{ eV} \quad (3b)$$
$$\rightarrow O^+ + D_2O, \quad \Delta H = 1.55 \pm 0.01 \text{ eV} \quad (4b)$$
$$\rightarrow D_2^+ + O_2, \quad \Delta H = 3.40 \pm 0.01 \text{ eV}. \quad (5b)$$

Finally, reactions (1c) through (5c) provide the heats of reaction for the product channels available with HD:

$$O_2^+ + HD \rightarrow OH^+ + OD, \quad \Delta H = 1.70 \pm 0.02 \text{ eV} \quad (1c')$$
$$\rightarrow OD^+ + OH, \quad \Delta H = 1.71 \pm 0.02 \text{ eV} \quad (1c'')$$
$$\rightarrow HO_2^+ + D, \quad \Delta H = 1.75 \pm 0.04 \text{ eV} \quad (2c')$$
$$\rightarrow DO_2^+ + H, \quad \Delta H = 1.66 \pm 0.09 \text{ eV} \quad (2c'')$$
$$\rightarrow HDO^+ + O, \quad \Delta H = 0.59 \pm 0.01 \text{ eV} \quad (3c)$$
$$\rightarrow O^+ + HDO, \quad \Delta H = 1.59 \pm 0.01 \text{ eV} \quad (4c)$$
$$\rightarrow HD^+ + O_2, \quad \Delta H = 3.37 \pm 0.01 \text{ eV}. \quad (5c)$$

Hereafter, we refer to the general process of reaction (1a), (1b), or (1c) as reaction (1), and likewise for processes (2)–(5).

II. EXPERIMENT

The ion-beam apparatus and experimental techniques used in this work are described in detail elsewhere.[20] Ions are produced as described below, mass analyzed in a magnetic sector, and decelerated to the desired translational energy. The ion beam is then injected into an rf octopole ion-beam guide, which passes through the reaction cell containing the neutral reactant gas. The pressure of the neutral gas is maintained sufficiently low to provide single-collision conditions. The unreacted and product ions drift out of the gas chamber to the end of the octopole, where they are extracted and analyzed in a quadrupole mass filter. Finally, ions are detected by a secondary electron scintillation ion counter using standard pulse counting techniques. Conversion of the raw ion intensities to total absolute reaction cross sections and individual product cross sections was described previously.[20] Except as noted below, the estimated uncertainty in the absolute cross sections is ±20%, while that of the relative cross sections is ±5%–10%.

The absolute energy scale and distribution of ion kinetic energies are determined by using the octopole beam guide as a retarding potential analyzer.[20] Typical full widths at half maximum in the ion kinetic energy distributions are 0.4 to 0.8 eV (lab), and the uncertainty in the absolute energy scale is ±0.05 eV (lab). Laboratory energies are converted to the center-of-mass (CM) frame of reference by using the formula, $E(\text{CM}) = E(\text{lab})M/(m+M)$ where m and M are the masses of the ion and neutral reactants, respectively. The conversion factors used here are 0.0593, 0.0863, and 0.112 for the H_2, HD, and D_2 reactions, respectively.

Studies were performed with O_2^+ ions made in two different ways. In early studies, an electron impact/drift cell (EI/DC) source was used. Although ionization of molecular oxygen is the most convenient source gas, both ground-state $O_2^+(X\,^2\Pi_g)$ and metastable $O_2^+(a\,^4\Pi_u)$ ions (lying 4.03 eV above the ground state[21]) are produced at electron energies high enough to produce a reasonably in-

tense ion beam. These ions can also be rotationally and vibrationally excited. Furthermore, direct electron impact of oxygen is impractical, because it oxidizes and destroys the ionization filament within a few hours. In contrast, the ionization filaments last for days if we ionize CO_2 by electron impact at an electron energy of 50 to 60 V. The resulting ions, CO_2^+, O^+, CO^+, and O_2^+ in ratios of ~100:10:2:1, are injected into a 20 mm long high-pressure drift cell[22] containing O_2 and Ar at partial pressures of 100–120 and 140–180 mTorr, respectively. The majority of the O_2^+ ions emitted from this drift cell source are produced from reactive collisions within the drift region. We calculate that the ions undergo approximately 600 to 1000 collisions, which should serve to cool them to near the ground vibrational and electronic states.

To verify that these early results corresponded to ground state O_2^+, we recently reexamined these systems with O_2^+ ions formed in a flow tube (FT) ion source.[23] This 1 m long flow tube operates at a pressure of 0.4–0.7 Torr with a helium flow rate of 3500–7000 standard cm^3/min. In this source, He^+ and He* are formed by microwave discharge. Further downstream, these species interact with O_2 to form O_2^+ ions [IE = 12.071 ± 0.001 eV (Refs. 21 and 24)] through charge transfer or Penning ionization. When the flow tube was operated with low pressures of O_2 added, experimental results that showed extensive internal excitation of the O_2^+ reactant ions were obtained. As the O_2 pressure was increased, the O_2^+ ions are cooled primarily by self-quenching collisions with the O_2 reagent gas. We have previously demonstrated that under these conditions this source produces O_2^+ ion beams that are >99.9% ground $O_2^+(X\,^2\Pi_g, v=0)$.[25] The results obtained with this source agree well with the best data obtained with the EI/DC source.

Commercially supplied H_2 and D_2, 99.99% purity, is used. HD gas is synthesized by standard methods[26] and has a purity of greater than 96%, as determined by mass spectrometric and Raman spectroscopic analyses. The impurities are H_2 and D_2 in approximately equal amounts. No corrections for these impurities are applied to the data.

III. RESULTS

A. Reaction of ground state $O_2^+(X\,^2\Pi_g, v=0)$

Reaction of $O_2^+(X\,^2\Pi_g)$ with H_2 (D_2, HD) results in production of OH^+ (OD^+), HO_2^+ (DO_2^+), H_2O^+ (D_2O^+, HDO^+), and O^+, processes (1)–(4). The reaction cross sections σ from representative data sets are shown as a function of translational energy, E, in Figs. 1–3. Figure 2 shows that the results for H_2 and D_2 are the same within experimental uncertainty. (The discrepancy between the cross sections for OH^+ and OD^+ is unlikely to be real. The cross section for OH^+ has a large uncertainty because this product ion is very close in mass to the much more intense H_2O^+ product ion. In the H_2 system, it was difficult to achieve conditions where both transmission and mass resolution could be optimized simultaneously.) Likewise, the total cross section in the HD system agrees with those for H_2 and D_2, although the distribution of products

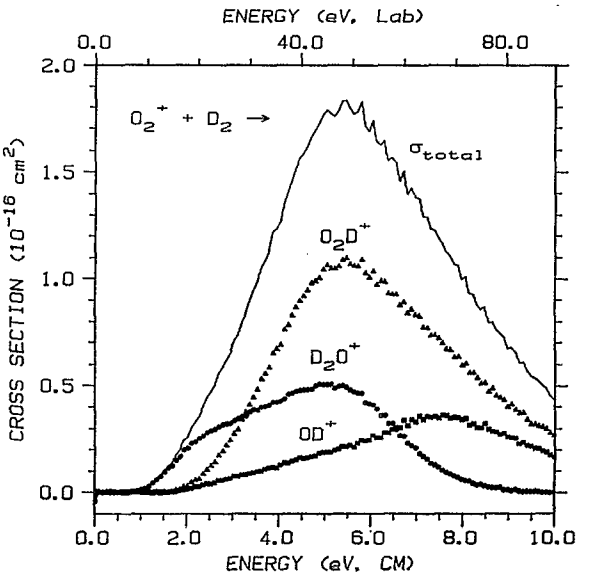

FIG. 1. Variation of product cross sections for reaction of $O_2^+(X\,^2\Pi_g)$ with D_2 as a function of translational energy in the laboratory frame of reference (upper scale) and the center-of-mass frame (lower scale). Circles denote $\sigma(D_2O^+)$, triangles denote $\sigma(DO_2^+)$, squares denote $\sigma(OD^+)$, and the solid line shows σ(total).

now differs. This is discussed further in the next section. All observed cross sections exhibit a threshold energy, which indicates that the O_2^+ ion beam is pure ground-state $X\,^2\Pi_g$, because reaction of excited-state $O_2^+(a\,^4\Pi_u)$ with H_2 is efficient and exothermic.[3,4]

Examination of Figs. 1–3 shows that H_2O^+ (D_2O^+, HDO^+) formation is initially dominant due to a lower

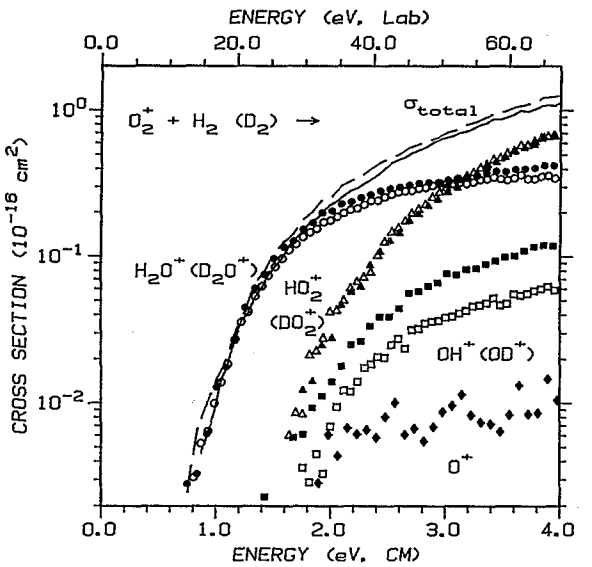

FIG. 2. Variation of product cross sections for reaction of $O_2^+(X\,^2\Pi_g)$ with H_2 (open symbols) and D_2 (solid symbols) as a function of translational energy in the laboratory frame of reference for H_2 (upper scale) and the center-of-mass frame for both systems (lower scale). Circles denote $\sigma(H_2O^+, D_2O^+)$, triangles denote $\sigma(HO_2^+, DO_2^+)$, squares denote $\sigma(OH^+, OD^+)$, and diamonds denote $\sigma(O^+)$. The solid and dashed lines denote σ(total) for the H_2 and D_2 systems, respectively.

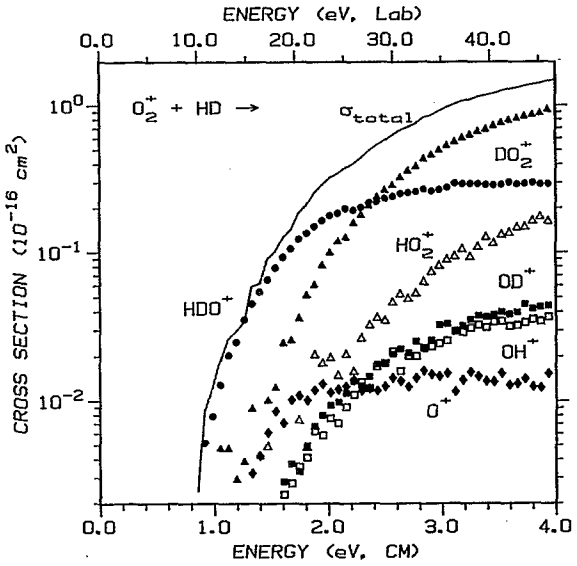

FIG. 3. Variation of product cross sections for reaction of $O_2^+(X\,^2\Pi_g)$ with HD as a function of translational energy in the laboratory frame of reference (upper scale) and the center-of-mass frame (lower scale). Circles denote $\sigma(HDO^+)$, open squares denote $\sigma(OH^+)$, solid squares denote $\sigma(OD^+)$, open triangles denote $\sigma(HO_2^+)$, solid triangles denote $\sigma(DO_2^+)$, and diamonds denote $\sigma(O^+)$. The total cross section is shown by the line.

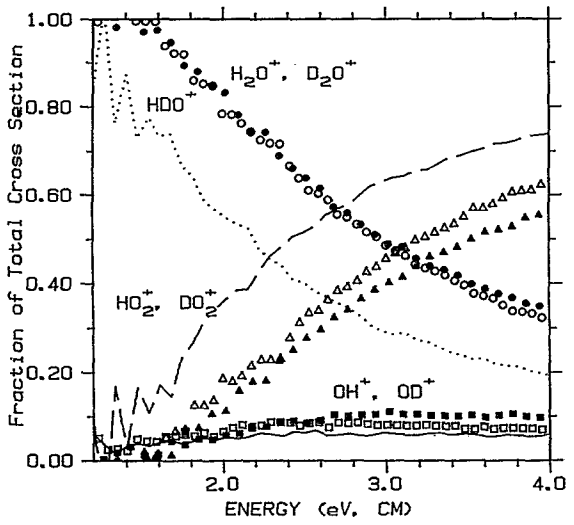

FIG. 4. Fractions of the total cross section for the three major product channels, $f(i)=\sigma(i)/\sigma(\text{total})$, as a function of kinetic energy in the center-of-mass frame. Open symbols correspond to reaction of $O_2^+(X\,^2\Pi_g)$ with H_2, solid symbols to reaction with D_2, and lines to reaction with HD. Squares and the solid line denote the fraction of reaction corresponding to process (1). Triangles and the dashed line denote the fraction of reaction corresponding to process (2). Circles and the dotted line denote the fraction of reaction corresponding to process (3).

threshold energy, but above about 3 eV, the HO_2^+ (DO_2^+) cross sections predominate. These results are only in partial agreement with the more qualitative measurements of Mahan and co-workers, who found that the H_2O^+ channel was of lower intensity than either the HO_2^+ or OH^+ channels at the lowest energy they studied, ~3 eV.

Both the H_2O^+ (D_2O^+, HDO^+) and HO_2^+ (DO_2^+) products reach maximum cross sections at about 5 eV (Fig. 1), suggesting competition with reaction (6),

$$O_2^+ + H_2 \rightarrow O_2^+ + H + H, \quad \Delta H = 4.478 \pm 0.001 \text{ eV} \quad (6)$$

and its isotopic analogs. OH^+ (OD^+) production is less efficient than reactions (2) and (3) at low energies, but becomes more significant at higher energies. This is because both the HO_2^+ (DO_2^+) and H_2O^+ (D_2O^+, HDO^+) products can decompose to form OH^+ (OD^+) in the overall process (7),

$$O_2^+ + H_2 \rightarrow OH^+ + O + H, \quad \Delta H = 6.13 \pm 0.01 \text{ eV}. \quad (7)$$

The OH^+ (OD^+) product formed in reaction (1) can in turn decompose to $H^+ + O$ or $O^+ + H$, beginning at 6.72 and 6.75 ± 0.01 eV, respectively. Some of the decline in the OD^+ and D_2O^+ cross sections observed at high energies in Fig. 1 may also be due to incomplete product collection, an experimental limitation that prevented obtaining accurate cross sections above ~4 eV CM in the H_2 and HD systems.

The intensity of the O^+ product ion is extremely small (Figs. 2 and 3), even though the energetics of process (4) are comparable to reactions (1) and (2). [The cross section for reaction (4) was not measured in the H_2 system due to the mass resolution constraints mentioned above.] This observation is consistent with previous results.[6] Attempts were made to measure the cross section for reaction (5a), but no H_2^+ was observed. The cross section for this process is likely to be small at the energies studied here, because the maximum energy examined, 4 eV, is only slightly above the threshold energy of 3.4 eV. Additionally, the experimental apparatus is not optimized in several respects for collection and detection of low-mass products, as discussed in detail elsewhere.[27] Thus, no further attempts were made to observe reaction (5b) or (5c).

B. Competition and kinetic isotope effects

Shown in Fig. 4 are the fractions of the total cross section attributed to the three main products, $f(i)=\sigma(i)/\sigma(\text{total})$. In all three systems, $f(OH^+,OD^+)$ is approximately constant and ranges from 0.06 to 0.10 ± 0.04 at kinetic energies greater than 2 eV. For the other two products, $f(H_2O^+,D_2O^+,HDO^+)$ decreases simultaneously and at approximately the same rate as $f(HO_2^+,DO_2^+)$ increases. Because the total cross sections are equivalent in all three systems, this shows that there is significant competition between product channels (2) and (3), and no apparent competition with channel (1).

Comparison of the cross section magnitudes for the HD system (Fig. 3) reveals an interesting intramolecular isotope effect. Specifically, above the threshold region, $\sigma(DO_2^+)/\sigma(HO_2^+)$ is about 6 ± 2 at 2 eV and decreases to 5 ± 1 between 4 and 5 eV. This observation concurs with previous results, in which the intensity of $\sigma(DO_2^+)$ exceeded that of $\sigma(HO_2^+)$ by factors of ~8 at 2 eV (Ref. 6) and ~7 at 2.6 eV.[5] This difference can be attributed in part to the lower threshold for reaction (2c″) compared with

process (2c'). For reaction (1), the ratio $\sigma(OD^+)/\sigma(OH^+)$ is nearly unity, as might be expected because the products differ only in the location of the charge. In addition, there appears to be an *inter*molecular isotope effect. As can be seen in Fig. 4, the simultaneous increase in $f(HO_2^+,DO_2^+)$ and decrease in $f(H_2O^+,D_2O^+,HDO^+)$ occurs far more rapidly for HD than for the H_2 and D_2 systems which exhibit comparable behavior. Specifically, $f(HO_2^+,DO_2^+)$ surpasses $f(H_2O^+,D_2O^+,HDO^+)$ at $\sim$3.1 eV with H_2 and D_2 and at only $\sim$2.3 eV with HD.

C. Threshold behavior

The threshold regions of the experimental reaction cross sections are analyzed by using the empirical model in Eq. (8),

$$\sigma(E)=\sigma_0(E+E_{\text{int}}-E_0)^n/E, \tag{8}$$

Here, E_0 is the translational threshold energy, E_{int} is the internal energy of the reactants ($=2kT=0.052$ eV for this system), σ_0 is an energy independent scaling factor, and n is a variable parameter. This model has been particularly useful in describing excitation functions of endothermic reactions and in deriving threshold energies.[28] Comparison of the model to the data is performed after convoluting Eq. (8) over the experimental kinetic energy distributions.[20] Optimum values for n, σ_0, and E_0 are found by using a nonlinear least-squares regression analysis.

In general, it is desirable to model the data over the widest possible energy range. The maximum energy is determined by the range of data taken, and by the onset of dissociative or competitive channels. Although the cross sections for reactions (1) and (2) could be modeled from threshold to 4 eV, the cross sections for process (3) could be modeled well from threshold to only 1.5–1.8 eV. This limited energy range is a result of the competition discussed above with the HO_2^+ (DO_2^+) channel, which begins at $\sim$1.7 eV. Instead of modeling the individual H_2O^+ (D_2O^+, HDO^+) cross sections, we model the sum of $\sigma(H_2O^+,D_2O^+,HDO^+)$ and $\sigma(HO_2^+,DO_2^+)$ to derive the optimized parameters. These same models also accurately describe the individual H_2O^+, D_2O^+, and HDO^+ cross sections from threshold to $\sim$1.5 eV.

Average results for σ_0, n, and E_0 for all channels are given in Table II. It can be seen that the optimized values of n lie in a small range of values, 1.4–2.2, for all reaction channels. For comparison, the thermodynamic thresholds calculated from literature thermochemistry are also listed in Table II. For both the HO^+ (DO^+) and HO_2^+ (DO_2^+) products, reactions (1) and (2), the experimental E_0 values agree with the literature values reasonably well. [The primary exception is for OD^+ formed in reaction (1c"), where the anomalously low threshold is due to a small amount of mass overlap from the HDO^+ product.] For the products of reaction (3), H_2O^+ (D_2O^+, HDO^+), the experimental values for E_0 are significantly above the thermodynamic values by an average of 0.50 ± 0.09 eV, well outside the uncertainties. An alternate way of examining this deviation is to note that if the literature values for E_0 are used in the model of Eq. (8), the experimental cross sections for reactions (1) and (2) are easily reproduced, but not those for reaction (3).

TABLE II. Comparison of modeled threshold energies to thermodynamic limits.[a]

Channel	σ_0	n	E_0 (eV)	Literature E_0 (eV)
(1a) OH^+ from H_2	0.19(0.02)	1.6(0.1)	1.70(0.03)	1.73(0.02)
(1b) OD^+ from D_2	0.16(0.08)	1.6(0.1)	1.69(0.09)	1.69(0.02)
(1c') OH^+ from HD	0.04(0.02)	1.4(0.2)	1.59(0.14)	1.70(0.02)
(1c") OD^+ from HD	0.06(0.01)	1.4(0.2)	1.41(0.10)	1.71(0.02)
(2a) HO_2^+ from H_2	0.67(0.18)	1.6(0.2)	1.93(0.13)	1.71(0.04)
(2b) DO_2^+ from D_2	0.46(0.08)	2.2(0.2)	1.80(0.08)	1.70(0.09)
(2c') HO_2^+ from HD	0.14(0.05)	1.9(0.1)	1.91(0.06)	1.75(0.04)
(2c") DO_2^+ from HD	0.66(0.10)	2.0(0.1)	1.64(0.03)	1.66(0.09)
(3a)[b] H_2O^+ from H_2	0.48(0.10)	2.2(0.2)	1.13(0.06)	0.62(0.01)
(3b)[b] D_2O^+ from D_2	0.38(0.11)	2.2(0.2)	0.98(0.08)	0.57(0.01)
(3c)[b] HDO^+ from HD	0.58(0.12)	2.2(0.2)	1.17(0.07)	0.59(0.01)

[a]Parameters of Eq. (8) as optimized with least-squares regression. Uncertainties are in parentheses.
[b]The sum of $\sigma(H_2O^+,D_2O^+,HDO^+)+\sigma(HO_2^+,DO_2^+)$ is modeled rather than $\sigma(H_2O^+)$, $\sigma(D_2O^+)$, or $\sigma(HDO^+)$, as discussed in the text.

The cross sections for reactions (4) were not analyzed in detail due to their very small size. It can be seen, however, in Figs. 2 and 3 that the apparent thresholds agree reasonably well with the literature thresholds listed above.

Overall, these analyses demonstrate that there are no activation barriers in excess of the endothermicities for reaction (1), (2), or (4), but there is for reaction (3). Based on these results alone, this barrier could lie either in the entrance or exit channel, but the electron impact ionization results of Foner and Hudson[9] suggest that it must lie in the entrance channel. The magnitude of the barrier measured here is just the average threshold found for reaction (3), 1.1 ± 0.1 eV. This is considerably less than that deduced by Mahan and co-workers, $\sim$2 eV,[6] and measured by Foner and Hudson, 2.5 ± 0.5 eV. The discrepancy between our work and the ionization studies of Foner and Hudson can be attributed to the sensitivity of the two methods. In the present work, no reaction is observed until this activation barrier is surmounted, and hence we are quite sensitive to this feature of the potential energy surface. In the ionization of H_2O_2, the barrier is measured by observing the onset for production of $O_2^+ + H_2$, a relatively minor channel compared with the other dissociation pathways of $H_2O_2^+$. This competition makes it much more difficult to observe the true threshold for $O_2^+ + H_2$ production. This point will be illustrated further below.

D. Reaction of internally excited O_2^+

It was not the intent of this work to study the excited states of O_2^+, largely because the identity of these states cannot be ascertained unequivocally. However, the results obtained were sufficiently interesting and in contrast to the results for ground state O_2^+ that they are also presented here.

As noted in the experimental section, excited O_2^{+*} ions are observed when low pressures of O_2 are introduced into

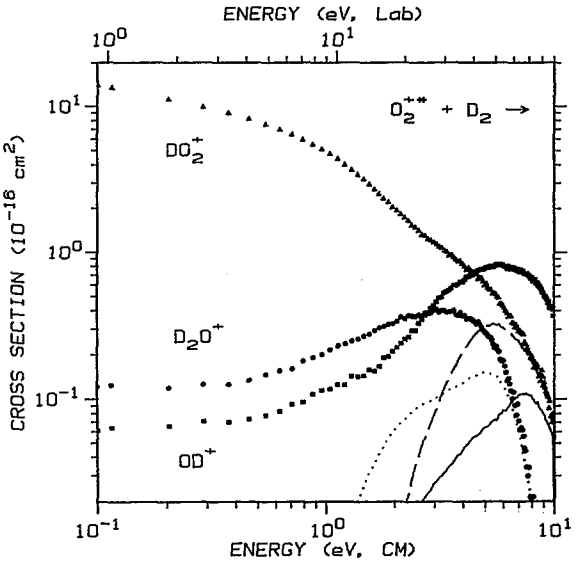

FIG. 5. Variation of product cross sections for reaction of excited O_2^+ (formed as described in the text) with D_2 as a function of translational energy in the laboratory frame of reference (upper scale) and the center-of-mass frame (lower scale). Circles denote $\sigma(D_2O^+)$, triangles denote $\sigma(DO_2^+)$, and squares denote $\sigma(OD^+)$. Dotted, dashed, and solid lines, respectively, show the cross sections for these products formed by reaction of $O_2^+(X\,^2\Pi_g)$ multiplied by 0.3.

the flow tube. Figures 5 and 6 show results obtained under such conditions (although not identical O_2 flows) for reaction with D_2 and HD, respectively. (H_2^+ and HD^+ product ions were not examined for reasons discussed above, and the O^+ product was not collected in the D_2 system.) It is evident that excited states of O_2^+ are present, and that

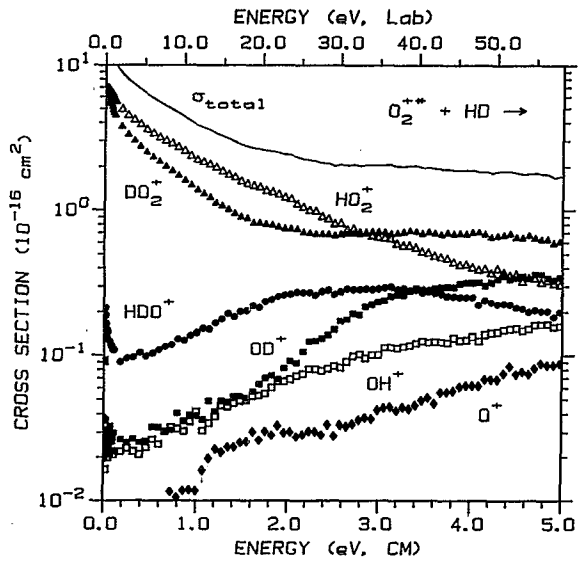

FIG. 6. Variation of product cross sections for reaction of excited O_2^+ (formed as described in the text) with HD as a function of translational energy in the laboratory frame of reference (upper scale) and the center-of-mass frame (lower scale). Circles denote $\sigma(HDO^+)$, open squares denote $\sigma(OH^+)$, solid squares denote $\sigma(OD^+)$, open triangles denote $\sigma(HO_2^+)$, solid triangles denote $\sigma(DO_2^+)$, and diamonds denote $\sigma(O^+)$. The total cross section is shown by the line.

such excitation must exceed the threshold for reaction (2). This means that it is either electronic excitation or excited vibrational levels of the $O_2^+(X\,^2\Pi_g)$ state where $v \geqslant 7$.

There is good reason to believe that electronic excitation dominates in these experimental results. First, if the excitation is electronic, then the only likely excited state present is the $a\,^4\Pi_u$ metastable, first excited state of O_2^+, 4.03 eV above the ground state.[21] Other excited states are known to rapidly radiate to either the $X\,^2\Pi_g$ or $a\,^4\Pi_u$ states.[29,30] Second, several studies have shown that $O_2^+(a\,^4\Pi_u)$ reacts efficiently with H_2 at thermal energies to form HO_2^+ and H_2^+ with no OH^+ or H_2O^+ observed.[2–4] Third, the TESICO (threshold-electron–secondary-ion coincidence) results of Tanaka *et al.*[5] show a strong enhancement in the production of HO_2^+ for reaction of $O_2^+(a\,^4\Pi_u)$ compared with $O_2^+(X\,^2\Pi_g, v=19,20)$, even though these states are nearly isoenergetic. Fourth, Tanaka *et al.* find that when $O_2^+(a\,^4\Pi_u)$ reacts with HD, the HO_2^+ product is favored over DO_2^+, in direct contrast to the results obtained for reaction of $O_2^+(X\,^2\Pi_g)$ with HD. In all cases, these results are consistent with those shown in Figs. 5 and 6.

A more quantitative assessment of the probable populations of states can also be made. Comparison of the absolute cross sections for reaction of D_2 with $O_2^+(X\,^2\Pi_g)$ and O_2^{+*} show that the latter are about $30\pm10\%$ of the former at the highest kinetic energies measured. This is illustrated in Fig. 5. This suggests that the O_2^{+*} beam contains about $30\pm10\%$ ground state ions (although the effects of vibrational excitation in the ground state on this analysis are unknown). We can estimate the fraction of $a\,^4\Pi_u$ state in the beam by examining the efficiency of reaction (2). Comparison of the cross section for production of DO_2^+ at low kinetic energies finds that it is about $36\pm7\%$ of the Langevin–Gioumousis–Stevenson (LGS) collision rate.[31] Previous work has found that the formation of $HO_2^+ + H$ in the reaction of $O_2^+(a\,^4\Pi_u) + H_2$ proceeds at about $56\pm17\%$ of the LGS collision rate (85% of the total reaction rate of $1.0\pm0.3\times10^{-9}$ cm^3 s^{-1} compared with a LGS collision rate of 1.52×10^{-9} cm^3 s^{-1}) (Ref. 4) and $63\pm26\%$ ($\sim$80%, as estimated from data shown in Fig. 10 of Ref. 3, of the total reaction rate of $1.2\pm0.5\times10^{-9}$ cm^3 s^{-1}).[3] These results suggest that the amount of $a\,^4\Pi_u$ in our beam is about $60\pm25\%$ (the average of 36/56 and 36/63). This is consistent with the independent estimate for the ground-state population made above.

Given the assignment of the reactivity observed in Figs. 5 and 6 to the $a\,^4\Pi_u$ state of O_2^+, there are several observations of interest in these figures. Because this state lies 4.03 eV above the ground state, reactions (1)–(5) are all exothermic, but only the HO_2^+ (DO_2^+) and H_2^+ products have been observed at thermal or near-thermal energies.[2–5] The present results find very small amounts of reactions (1), (3), and (4), consistent with the failure to observe these products previously. Although it is possible that these products are formed by small amounts (10%–20%) of high vibrational levels of $O_2^+(X\,^2\Pi_g)$, the observations here suggest that these products have not been

observed previously in the reactions of $O_2^+(^4\Pi_u)$ because these channels exhibit barriers to reaction (Figs. 5 and 6). We speculate that the small increase in these cross sections at the lowest energies (Fig. 6) is due to vibrationally excited $O_2^+(a\,^4\Pi_u)$.

There are a couple of observations that tend to support the assignment of these minor products to reaction of $O_2^+(a\,^4\Pi_u)$. One is the large increase in OD^+ production observed in Figs. 5 and 6 at about 2 eV. This energy corresponds nicely to the endothermicity of reaction (7), the decomposition of HO_2^+ and H_2O^+ to form OH^+, which is 2.10 ± 0.01 eV for reaction of the $O_2^+(a\,^4\Pi_u)$ state. Another is that $\sigma(DO_2^+)$ declines approximately as $E^{-0.5\pm0.1}$ at the lowest kinetic energies of 0.1–0.7 eV, but then begins to decline as $E^{-1.4\pm0.2}$ until about 5 eV, where it begins to fall off as $E^{-4\pm1}$. (The large error bars in the latter figure depend on whether the measured cross section is analyzed directly, E^{-3}, or whether it is first corrected for contributions from ground state O_2^+, E^{-5}.) The latter decline may correspond to decomposition by reaction (6), 4.478 eV if the $a\,^4\Pi_u$ state of O_2^+ is reformed. The break in the cross section at about 0.7 eV could also correspond to reaction (6), endothermic by 0.45 eV if the $X\,^2\Pi_g$ state of O_2^+ is formed. An alternative explanation for the break at 0.7 eV comes from a simple model for conservation of angular momentum in exothermic reactions. Outlined in detail elsewhere,[32] this model predicts that the cross section for reaction (2b) is restricted by angular momentum considerations beginning at 0.76 eV for a reaction that is exothermic by 2.33 eV, the calculated thermochemistry for reaction of $O_2^+(a\,^4\Pi_u)$. This is plausible evidence that the DO_2^+ reaction does indeed correspond to this state of O_2^+. This assignment can be tested by examining the cross sections for HO_2^+ and DO_2^+ in the HD system. The angular momentum model predicts critical energies of 1.55 and 0.29 eV, respectively, whereas reaction (6) is endothermic by 0.49 eV for both products. The data of Fig. 6 clearly show that $\sigma(DO_2^+)$ declines more rapidly than $\sigma(HO_2^+)$ in qualitative agreement with the angular momentum model, although the breaks in these cross sections are not predicted as quantitatively as in the D_2 system. This may be a reflection that both reaction (6) and the angular momentum restriction are involved in the declines observed in the cross sections for reactions (2c′) and (2c″).

IV. DISCUSSION

A. Reaction mechanisms and molecular orbital correlations

To understand the origins of the activation barrier for the reaction of $O_2^+ + H_2$, we need to consider the mechanism and potential energy surfaces in more detail. Simple consideration of the reaction mechanism suggests that there must be two intermediates involved. The most stable intermediate is likely to be ionized hydrogen peroxide, I, which can be formed by an approach of O_2^+ and H_2 where the bonds are parallel. This intermediate can decompose easily to form $OH^+ + OH$ or $HO_2^+ + H$. Formation of $H_2O^+ + O$ and $H_2O + O^+$ seems likely to proceed via intermediate II, formed by a perpendicular approach of O_2^+ and H_2. II can also decompose to $HO_2^+ + H$:

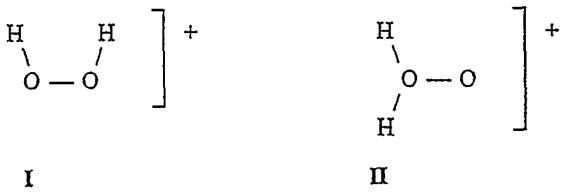

I II

To understand why there is a barrier to formation of these intermediates, we examine molecular orbital (MO) correlation diagrams for the interactions of O_2^+ with H_2. To construct these diagrams, we adapt and extend Mahan's original MO diagram for an $[H\text{–}A\text{–}A\text{–}H]^+$ system (where A is any atom) to produce $HA_2^+ + H$, as well as a diagram for producing HO_2^+ from a nonlinear $[O\text{–}O\text{–}H\text{–}H]^+$ intermediate, and a diagram for forming $HCO^+ + H$ from ionized formaldehyde.[8] Mahan did not discuss the $OH^+ + OH$, the $H_2O^+ + O$, or the $H_2O + O^+$ product channels, nor did he consider intermediate II.

To generate such MO diagrams, the relative energies of the highest occupied and lowest unoccupied electron orbitals are required. Those for the reactants and HO_2, H, and OH species are available from Mahan.[8,33] For the H_2O and O species, the relative energies of the highest occupied $1b_1(H_2O)$ and $2p(O)$ levels are derived from the ionization energies.[21] The remaining orbitals are approximated, as are the relative energies of the MO's of the intermediates. Any uncertainty in the exact position of the orbitals is unlikely to affect the qualitative conclusions. Correlations between the orbitals of the reactants and intermediates are determined by using the nodal structure of the evolving MO's in C_s symmetry.[8] The ground-state (GS) occupation for the reactant orbitals is shown along with the adiabatic correlation of these electrons to the intermediate orbitals.

Figure 7 shows the correlation diagram for formation of intermediates I and II from the reactants. The symmetry of the orbitals in C_{2v} symmetry is indicated with the primary source of each orbital denoted in brackets. As noted by Mahan, the adiabatic evolution of the reactant orbitals to the $HOOH^+$ intermediate is such that the doubly occupied $\sigma_g(H_2)$ orbital evolves to an antibonding $\sigma^*(OH)$ orbital in $HOOH^+$. (Indeed, Mahan places the energy of this orbital above those of the $b_2[\sigma^*(OH)]$ and $b_2[\sigma^*(O_2)]$ MO's, but this does not affect the overall correlations and so the energy of this orbital is chosen for clarity.) Mahan considered a C_{2v} symmetry approach of O_2^+ and H_2, but this symmetry cannot be maintained in any real collision. Because even a plane of symmetry is unlikely in a real collision, the appropriate symmetry to consider is C_1 symmetry. Now, there will be an interaction between the MO evolving from the $\sigma_g(H_2)$ orbital and those evolving from the $\pi_g^*(O_2)$ orbitals to nonbonding $n(O_2)$ and antibonding $\pi^*(O_2)$ orbitals of the intermediate. Mahan suggested that the remnants of these avoided crossings constitute the barrier to formation of $HOOH^+$ from $O_2^+ + H_2$. Examination of the left side of Fig. 7 shows that nearly identical con-

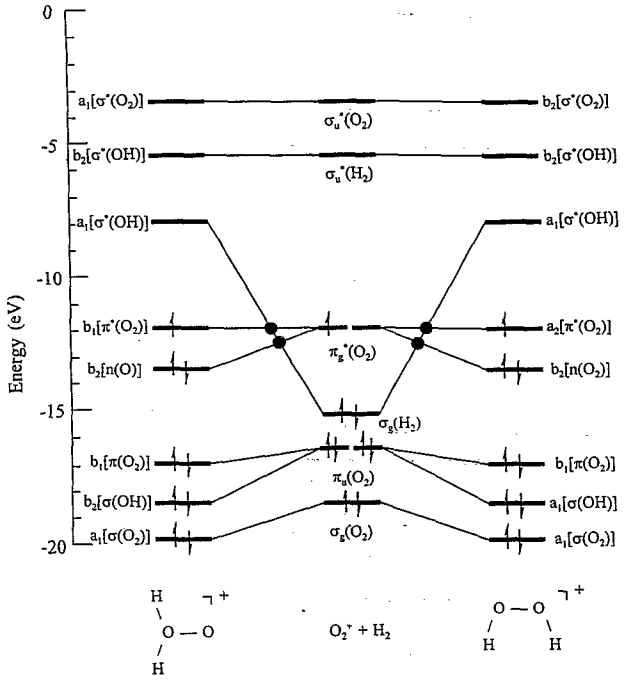

FIG. 7. Molecular orbital correlation diagram in C_{2v} symmetry for production of intermediates I and II from $O_2^+(X\,^2\Pi_g)+H_2(^1\Sigma_g^+)$ reactants. Orbital energies are given along the vertical axis. The solid lines show diabatic correlations in C_{2v} symmetry, while the circles show crossings that become avoided in C_1 symmetry. The electrons, denoted by arrows, show the ground-state occupations of the reactants and the adiabatic correlation of these electrons to the orbitals of the intermediates.

siderations hold for formation of intermediate II (where again the energy of the $a_1[\sigma^*(OH)]$ MO could be much higher). In retrospect, it probably should come as no surprise that there is a potential energy barrier when the doubly occupied $\sigma_g(H_2)$ orbital approaches the occupied orbitals of O_2^+.

Another feature of the interaction of $O_2^+ + H_2$ that has not been commented on previously to our knowledge is also evident from Fig. 7. This involves where the radical electron that begins in the $\pi_g^*(O_2)$ orbital ends up in the intermediates. Figure 7 shows that after the avoided crossings are considered, the two $\pi_g^*(O_2)$ orbitals adiabatically evolve to a $\pi^*(O_2)$ orbital and to a strongly antibonding $a_1[\sigma^*(OH)]$ orbital for either intermediate. If the π^*-like orbital is occupied, then the ground state of either intermediate is formed. If the $a_1[\sigma^*(OH)]$ orbital ends up being occupied, however, an excited state of the intermediates is generated. The energy of this a_1 orbital is likely to be sufficiently high in energy that this excited intermediate is *not* an important path for reaction.

The consequences of this can be seen by considering the possible surface symmetries and the possible states of the intermediate that can be formed from the reactants and various product channels. This is achieved by consideration of spin and angular momentum correlation rules[34] and the results for interaction in C_s symmetry are given in Table III. Two doublet surfaces, $^2A'$ and $^2A''$, are available to the reactant channel $O_2^+(X\,^2\Pi_g)+H_2(^1\Sigma^+)$, as also indicated by the more complete correlation diagram. Likewise, the $OH^+ + OH$ and $H_2O^+ + O$ product channels can form both a $^2A'$ and a $^2A''$ intermediate, while the $HO_2^+ + H$ and $H_2^+ + O_2$ product channels can form only the $^2A''$ ground-state intermediate. Although all four product channels can also form intermediates of quartet spin, these are considered unimportant because formation of such intermediates from ground-state reactants is spin forbidden. Finally, Table III shows that the $O^+(^4S) + H_2O(^1A_1)$ product channel correlates only with a quartet intermediate and hence is a spin-forbidden reaction channel, explaining its inefficiency. Overall, we conclude that the reaction of O_2^+ with H_2 is likely to occur on a single surface of doublet spin via a $^2A''$ intermediate.

TABLE III. Spin and angular momentum correlations.

Channel	Term symbol[a]	C_s symmetry	Intermediate	Surfaces[b]
$O_2^+ +$ H_2, D_2, HD	$^2\Pi_g$ $^1\Sigma_g^+(^1\Sigma^+)$	$^2A'+{}^2A''$ $^1A'$	$^2A'+{}^2A''$	4(2)
$O^+ +$ H_2O, D_2O (HDO)	^4S_u $^1A_1(^1A')$	$^4A''$ $^1A'$	$^4A''$	0(0)
OH^+, $OD^+ +$ OH, OD	$^3\Sigma^-$ $^2\Pi$	$^3A''$ $^2A'+{}^2A''$	$^{2,4}A'+{}^{2,4}A''$	4(2)
H_2O^+, D_2O^+ (HDO$^+$) $+O$	$^2B_1(^2A'')$ ^3P_g	$^2A''$ $^3A'+(2)^3A''$	$^{2,4}A''+(2)^{2,4}A'$	4(2)
HO_2^+, DO_2^+ $+H$, D	$^3A''$ ^2S_g	$^3A''$ $^2A'$	$^{2,4}A''$	2(2)
$H_2^+ +$ O_2	$^2\Sigma_g^+$ $^3\Sigma_u^-$	$^2A'$ $^3A''$	$^{2,4}A''$	2(2)

[a]Terms in parentheses correspond to the HD and HDO^+ species.
[b]Maximum number of reactive surfaces for reactions (1)–(5). The number in parentheses assumes that only the ground state $^2A''$ intermediate is important.

More detailed MO correlation diagrams for intermediates I and II evolving to the products of reactions (1)–(3) were also constructed, but are not shown here for brevity. These diagrams indicate that the ground-state $^2A''$ intermediates can smoothly evolve to ground-state $OH^+ + OH$ and ground-state $H_2O^+ + O$ products. In C_s symmetry, neither intermediate correlates with ground-state $HO_2^+(^3A'')+H(^2S)$ products, but rather to $H^+(^1S) + HO_2(^2A'')$, 2.25 eV higher in energy. However, the doublet surfaces evolving from these two product channels will have an avoided crossing in C_1 symmetry, such that $HO_2^+ + H$ can be formed from either intermediate I or II, although there is the possibility of a bottleneck along the potential energy surface leading to this product.

Reaction of $O_2^+(a\,^4\Pi_u)$. The correlation diagram shown in Fig. 7 can also be applied to the reaction of $O_2^+(a\,^4\Pi_u)$, as previously noted by Mahan.[8] The orbital configuration for this state, $\sigma_g^2\pi_u^3\pi_g^2$, necessarily leads to occupation of the antibonding $a_1[\sigma^*(OH)]$ orbital of both intermediates I and II. It is also worth noting that the hole

in the occupation of the $\pi_u(O_2)$ orbital leads to a hole in the bonding electrons of the intermediates, either $\sigma(OH)$ or $\pi(O_2)$. Thus, $O_2^+(a\,^4\Pi_u)+H_2(^1\Sigma_g^+)$ reactants correlate with an excited quartet state of the intermediates. The lowest-lying quartet state of the intermediates correlates instead to $O_2(^3\Sigma_g^-)+H_2^+(^2\Sigma_g^+)$, an asymptote that lies 0.7 eV lower in energy. Clearly, it will be very difficult for the $O_2^+(a\,^4\Pi_u)+H_2(^1\Sigma_g^+)$ reactants to form a long-lived intermediate. Indeed, Henglein and co-workers[7] have found that reaction (2) is direct for this state. This is also consistent with the apparent barriers to reactions (1) and (3) observed in Figs. 5 and 6.

B. Phase space theory calculations

Because of the activation barrier in the entrance channel for the interaction of $O_2^+(X\,^2\Pi_g)$ with H_2, phase space theory (PST) cannot be directly applied to this reaction. However, the crossed beam studies of Mahan and co-workers indicate that the products of reactions (1)–(3) proceed via a long-lived intermediate at energies below about 5 eV.[6] Thus, PST should be capable of describing the branching ratios between these products. This application of PST may not be completely quantitative, however, because the angular momentum of the intermediate formed by passing over the tight transition state in the entrance channel will differ from that for the "loose" transition state assumed by PST. Nevertheless, the comparison of a PST calculation to our data is edifying.

In PST calculations, reactions are assumed to proceed through a strongly coupled intermediate, while total angular momentum and energy are explicitly conserved. Programs from Chesnavich and co-workers were adapted to perform the present calculations.[10] Here, loose transition states are assumed, a classical treatment is employed, and all nonlinear molecules are approximated as spherical tops.[35] A further approximation is used to simplify the treatment of linear species.[16] Table IV shows the molecular constants for reactants and products used in these calculations. All vibrational degrees of freedom are treated as anharmonic oscillators, and the anharmonicities $\omega_e x_e$ are calculated according to a Morse potential.[36] Constants ω_e and B for the diatomic species are taken from Huber and Herzberg.[37] Rotational constants for HO_2^+ and DO_2^+ are derived from structure calculations by Raine, Schaefer, and Handy,[38] and vibrational constants are determined from these calculations and photoelectron spectra measured by Dyke *et al.*[39] Constants for H_2O^+, D_2O^+, and HDO^+ are taken from calculations by Botter and Carlier.[40] Table V provides additional parameters needed for each reaction channel. The symmetry number listed is the product of symmetry numbers for the ionic and neutral species.

Determination of the phase space available to each reaction channel must account for the degeneracy of the electronic states. However, as Herbst and Knudson have pointed out, it is possible and necessary to exclude from the statistical sum those states that have barriers or are otherwise inaccessible.[41] This is accomplished by including for each channel i the number of reactive potential surfaces,

TABLE IV. Molecular constants (in cm^{-1}) used in phase space calculations.

Species	ω_e [a] ($\omega_e x_e$)[b]	B [a,c]
O_2^+	1905 (16.6)	1.69
H_2	4401 (126.4)	60.85
D_2	3116 (63.4)	30.44
HD	3813 (94.9)	45.66
OH	3738 (93.5)	18.91
OH^+	3113 (57.3)	16.79
OD	2720 (49.5)	10.02
OD^+	2272 (30.5)	8.91
HO_2^+	1566[d] (25), 3204[e] (110), 1144[e] (15)	2.05[e]
DO_2^+	1580[d] (25), 2360[e] (57), 870[e] (8)	1.61[e]
H_2O^+ [f]	3190 (56), 3300 (60), 1405 (11)	13.93
D_2O^+ [f]	2320 (30), 2400 (32), 1060 (6)	6.98
HDO^+ [f]	3200 (56), 2400 (32), 1225 (8)	9.30
$H_2O_2^+$ [g]	3610, 3610, 1350, 1266, 1040	1.90
$D_2O_2^+$ [g]	2660, 2660, 1040, 1015, 947	1.43
HDO_2^+ [g]	3610, 2660, 1310, 1040, 980	1.61

[a]Vibrational constants ω_e and rotational constants B for diatomic species are taken from Ref. 37.
[b]Anharmonicity constant calculated assuming a Morse potential (Ref. 36).
[c]For nonlinear species, the rotational constant B is $h/(4\pi cI)$, where I is approximated as $(I_A I_B I_C)^{1/3}$.
[d]Constant for O–O stretch is taken as the average of the values measured in Ref. 39 and calculated in Ref. 38. Uncertainty is 50 cm^{-1}.
[e]Structure and ω_e taken from Ref. 38. Uncertainty is 50 cm^{-1} in ω_e. Structure of DO_2^+ is assumed to be that of HO_2^+ for calculation of B.
[f]Structure and ω_e taken from Ref. 40. Uncertainty is 20 cm^{-1} in ω_e.
[g]All values taken from Ref. 43 except for the O_2 stretching frequency of 1040 cm^{-1}. This was increased from the 880 cm^{-1} value in all three neutral molecules in accord with the increase in the vibrational frequency of O_2^+ vs O_2. Anharmonicities are ignored.

TABLE V. Parameters used in phase space calculations.

Reaction channel		Reduced mass (amu)	Polarizability (Å^3)	Symmetry number[a]
$O_2^+(X\,^2\Pi_g)$	$+H_2(^1\Sigma_g^+)$	1.897	0.790[b]	4
	$+D_2(^1\Sigma_g^+)$	3.578	0.775[b]	4
	$+HD(^1\Sigma^+)$	2.761	0.783[b]	2
$OH^+(^3\Sigma^-)$	$+OH(^2\Pi)$	8.504	1.1[c]	1
	$+OD(^2\Pi)$	8.748	1.1[c]	1
$OD^+(^3\Sigma^-)$	$+OD(^2\Pi)$	9.007	1.1[c]	1
	$+OH(^2\Pi)$	8.748	1.1[c]	1
$HO_2^+(^3A'')$	$+H(^2S_g)$	0.978	0.667[d]	1
	$+D(^2S_g)$	1.898	0.67[e]	1
$DO_2^+(^3A'')$	$+D(^2S_g)$	1.901	0.67[e]	1
	$+H(^2S_g)$	0.979	0.667[d]	1
$H_2O^+(^2B_1)$	$+O(^3P_g)$	8.474	0.802[d]	2
$D_2O^+(^2B_1)$	$+O(^3P_g)$	8.894	0.802[d]	2
$HDO^+(^2A'')$	$+O(^3P_g)$	8.690	0.802[d]	1

[a]Product of the symmetry numbers for the ionic and neutral species.
[b]J. O. Hirschfelder, C. R. Curtiss, and R. B. Bird, *Molecular Theory of Gases and Liquids* (Wiley, New York, 1954), p. 947.
[c]$\alpha(OH)$ is estimated using the empirical method of K. J. Miller and J. A. Savchik, J. Am. Chem. Soc. **101**, 7206 (1979). $\alpha(OD)\approx\alpha(OH)$ is assumed.
[d]T. M. Miller and B. Bederson, Adv. At. Mol. Phys. **13**, 1 (1977).
[e]$\alpha(D)\approx\alpha(H)$ is assumed.

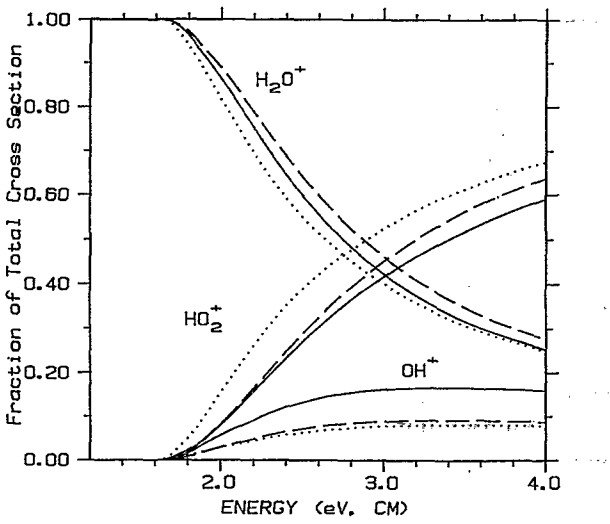

FIG. 8. Fractions of the total cross section for the three major product channels, $f(i)=\sigma(i)/\sigma(\text{total})$, as a function of kinetic energy in the center-of-mass frame. Solid lines correspond to the results of phase space calculations with the parameters given in Tables IV and V. Dashed lines show results of phase space calculations where the magnitude of the OH^+ channel has been restricted by a factor of 2. Dotted lines correspond to the translationally driven reaction theory calculations described in the text.

$g(i)$. In the case of the reactant channel only, the *total* number of available surfaces must be included as well. Based on the information in Table III and the considerations discussed above, one of two doublet reactant surfaces is considered to be reactive, and the product channels for reactions (1)–(3) are accessible along this surface.

The results of these calculations are shown in Fig. 8 and can be compared directly to Fig. 4. Qualitatively, the PST calculations reproduce the strong competition between reactions (2) and (3) and also the relative inefficiency of reaction (1). This agreement implies that the assumptions of PST hold for these reactions; namely, that all three reaction channels proceed through long-lived intermediate complexes at these energies, in agreement with the crossed beam results. (We note, however, that Mahan and co-workers attributed the inefficiency of the $H_2O^+ + O$ channel relative to the $HO_2^+ + H$ channel to some dynamic constraint. The present PST results show that the dominance of the $HO_2^+ + H$ channel is statistically governed, and can be traced to the lower vibrational frequencies and rotational constant of the latter channel.) An improvement in the quantitative agreement between the PST and experimental results can be achieved by halving the calculated cross sections for reaction (1). This can be thought of as a reduction in the number of accessible surfaces, as an increase in the symmetry number of the channel (from one to two), or as a reflection of some constraint in the reaction that is not directly considered by PST. An example of the latter could be the relative population of intermediates I and II, because reaction (1) arises only from I while II can lead to reactions (2) and (3).

Phase space calculations for the D_2 reaction system are similar to those shown for H_2, although the energy at which $f(DO_2^+)=f(D_2O^+)$ is shifted up by about 1 eV. Thus, PST does not reproduce the similar behavior observed between the H_2 and D_2 systems (Fig. 2), a result that could be due to the inexact treatment of the angular momentum of the intermediate. PST calculations for the HD system were also performed and yield similar results to those shown in Fig. 8. [The energy at which $f(HO_2^+ + DO_2^+)=f(HDO^+)$ is now intermediate between those energies for the H_2 and D_2 systems.] The calculations find that the amount of $OH^+ + OD$ is exactly the same as $OD^+ + OH$, in agreement with the experimental results (Fig. 3). The PST results also find that $DO_2^+ + H$ is favored over $HO_2^+ + D$ by a factor of about 1.5, considerably less than the experimental ratio. This suggests that the strong enhancement of the $DO_2^+ + H$ product channel has a dynamic as well as a statistical explanation.

Reaction of $O_2^+(a\,^4\Pi_u)$. Because the reaction of the $a\,^4\Pi_u$ state is primarily a direct one, phase space calculations are not an appropriate way of analyzing these results. Nevertheless, PST calculations performed on this system provided some interesting results. Not surprisingly, if the thresholds for reactions (1)–(3) are lowered by the excitation energy of the $a\,^4\Pi_u$ state, the production of OH^+ and H_2O^+ are much larger than observed experimentally. If the thresholds for these two channels are arbitrarily increased, better agreement can be obtained. In particular, we found that if the exothermicity of reaction (1) was set to about 0.4 eV, the magnitude and shape of the OD^+ cross section in Fig. 5 could be reproduced rather nicely. This result indicates that the barrier to reactions (1) and (3) need not *exceed* the energy of the $O_2^+(a\,^4\Pi_u) + D_2$ reactants because the competition with reaction (2) can surpress the probability of these processes at low energies.

C. Translationally driven reaction theory

Phase space theory cannot include the effects of the tight transition state in the entrance channel; however, a modified theory developed by Marcus[18] and reformulated by Chesnavich and Bowers[17] can include such a feature. This theory states that the translational energy (E_t) dependence of the cross section for a particular reaction channel α is given by

$$\sigma_\alpha(E_t)=(\pi\hbar^2/2\mu E_t)\int_0^{J_{\max}} P(E_t,J)R_\alpha(J)2J\,dJ, \quad (9)$$

where μ is the reduced mass of the reactants and J is the total angular momentum. $R_\alpha(J)$ is the relative probability for decomposition of the intermediate complex into product channel α and is given by $k_\alpha(E,J)/\Sigma k_i(E,J)$, where the k's are the unimolecular rate constants for decomposition and the summation is over all channels. The reaction probability term $P(E_t,J)$ is given by $(1/2L)dW^\ddagger(E^\ddagger)/dL$, where L is the orbital angular momentum and $E^\ddagger=E_t-E_0-L^2B^\ddagger$ is the energy available to the transition state with E_0 being the height of the potential energy surface at the transition state and $B^\ddagger$ being the rotational constant of the transition state (treated as a spherical molecule). $W^\ddagger(E^\ddagger)$ is essentially the sum of states at the transition state of the

vibrational modes formed during creation of the transition state. The classical expression for $W^\ddagger(E^\ddagger)$ is $(C_r^\ddagger C_v^\ddagger / C_r C_v) E^{\ddagger(\Delta v+2)/2}/\Gamma[\Delta v/2 + 2]$ where Δv is the number of new vibrational degrees of freedom formed during creation of the transition state, Γ is the gamma function, and C_r and C_v are rotational and vibrational constants.

For the $O_2^+ + H_2$ reaction, $\Delta v = 3$, $C_r^\ddagger / C_r = \sigma B(O_2^+) B(H_2) \pi / \sigma^\ddagger B^{\ddagger 3/2}$, where σ and $\sigma^\ddagger$ are the symmetry numbers of the reactants and transition state, respectively, and $C_v^\ddagger / C_v = (\Pi h \nu_i^\ddagger)^{-1}$ where the product is over Δv vibrations. Thus, $W^\ddagger = (C_r^\ddagger C_v^\ddagger / C_r C_v) E^{\ddagger 5/2}/\Gamma(7/2)$. This classical expression can be quantized by noting that it is directly proportional to the classical expression for the density of states of a molecule with three vibrations and a one-dimensional rotor, $\rho_{3,1}(E^\ddagger)$. Hence, $W^\ddagger = [\sigma B(O_2^+) B(H_2)/\sigma^\ddagger B^\ddagger] \rho_{3,1}(E^\ddagger)$. In this work, this density of states was calculated by using the Whitten–Rabinovitch semiclassical expression.[42] Direct counting methods were also attempted but the discrete changes in the value of $W^\ddagger$ as a function of energy led to an ill-behaved function for $dW^\ddagger/dL$. The purely classical expression was also examined, but the semiclassical calculation agreed better with the experimental results.

In order to implement this expression, the only parameters now required are estimates of the vibrational frequencies $\nu^\ddagger$ and rotational constant $B^\ddagger$ of the transition state. The vibrational frequencies and average rotational constants for $H_2O_2^+$, $D_2O_2^+$, and HDO_2^+ (Table IV) were estimated by using the molecular constants for the neutral analogs given by Giguère and Liu,[43] and adjusting the O_2 stretching frequency to account for the increased bond strength in $H_2O_2^+$ vs H_2O_2. The low-frequency torsion mode was chosen as the reaction coordinate and anharmonicities were ignored. Molecular constants for the product channels were the same as for the PST calculations (Tables IV and V). The number of reactive surfaces was the single doublet surface for each channel and the symmetry number for the OH^+ (OD^+) channel was arbitrarily increased to two as outlined above. Endothermicities for all channels were taken as the literature values calculated above. The only remaining parameter is the height of the transition state barrier and this was set at 1.1 eV to match the experimental results.

The results of this calculation are shown in Figs. 8 and 9. Figure 8 shows that the branching ratio is very similar to the PST results. This should be the case because the R_α term in Eq. (9) is essentially equivalent to the phase space calculation, and the only difference is the distribution of angular momenta of the intermediate formed via a loose vs a tight transition state. The results shown in Fig. 9 are more impressive because they show that the theory reproduces not only the product branching ratios, but also the shape and absolute magnitudes of the experimental cross sections. Comparable agreement is obtained for the H_2 system. [The only major distinction between the H_2 and D_2 results is that cross section for HO_2^+ is somewhat larger than for DO_2^+ such that the energy where $\sigma(HO_2^+)$ equals $\sigma(H_2O^+)$ is lower in the H_2 system by about 0.5 eV. Note that this is less of a shift than in the phase space calculations.] Even better quantitative agreement between the experimental and theoretical results could be obtained by adjusting the vibrational frequencies and rotational constant of the transition states.

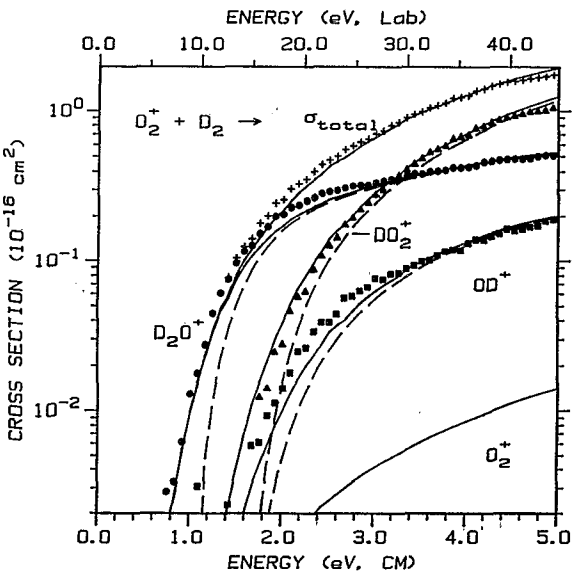

FIG. 9. Comparison of experimental results for $O_2^+(X\,^2\Pi_g) + D_2$ with translationally driven reaction theory calculations as a function of translational energy in the laboratory frame of reference (upper scale) and the center-of-mass frame (lower scale). Symbols show the experimental results, which are the same as shown in Figs. 1 and 2, although plus symbols now denote σ(total). Dashed lines show the theoretical calculations made as described in the text. Solid lines show these calculations convoluted over the experimental energy distributions.

Also shown in Fig. 9 is the calculated cross section for a return to reactants after formation of the intermediate. Although the true threshold for this channel is 1.1 eV, this cross section is small and rises slowly. This confirms that formation of $O_2^+ + H_2$ from directly ionized hydrogen peroxide is inefficient. These results demonstrate that an apparent threshold of 2.5 ± 0.5 eV for this process, as observed by Foner and Hudson,[9] is quite consistent with the present experimental and theoretical results. This theoretical result also shows why the conclusion of Mahan and co-workers[6] that the barrier height must be similar to the thresholds for HO_2^+ and OH^+ is incorrect. They concluded that this must be so because otherwise the intermediate complex "would simply redissociate to reactants over the low barrier between reactants and complex." The calculations demonstrate that the phase space associated with the tight transition state is appreciably less than that of the other product channels, and hence, low barrier or not, the intermediate complex does not dissociate back to reactants readily.

Theoretical results for the HD system were also calculated, but as in the phase space theory results, the ratio of DO_2^+ to HO_2^+ was only 1.5. Because the theory does not accurately predict the strong enhancement of the DO_2^+ channel, it does not accurately predict the absolute cross sections nor the branching ratios for the various product channels in the HD system. The energy dependence of the

various channels is accurately predicted, however, as in the results shown in Fig. 9. Again, this failure of the theoretical model suggests that dynamic constraints dominate the intramolecular isotope effect observed here.

V. SUMMARY

Guided ion-beam mass spectrometry has been used to study the reactions of $O_2^+(X\,^2\Pi_g)$ with H_2, D_2, and HD from thermal energies to over 4 eV. Four types of product ions are observed, namely OH^+ (OD^+), HO_2^+ (DO_2^+), H_2O^+ (D_2O^+, HDO^+), and O^+, although formation of the latter is very inefficient. All observed product channels show endothermic behavior, and analysis of the threshold behavior shows that the OH^+ (OD^+), HO_2^+ (DO_2^+), and O^+ product channels occur at the thermodynamic limit. However, a barrier to forming H_2O^+ (D_2O^+, HDO^+) is observed, and the O_2H_2 ionization results of Foner and Hudson[9] show that this barrier is in the entrance channel. Empirical modeling of the present results yields a barrier height of 1.1 ± 0.1 eV. In all systems, the dependence of the branching ratios as a function of energy shows that the mechanisms for forming HO_2^+ (DO_2^+) and H_2O^+ (D_2O^+, HDO^+) are intimately coupled. This coupling differs in the HD system, such that the energy at which $\sigma(HO_2^+, DO_2^+)$ exceeds $\sigma(H_2O^+, D_2O^+, HDO^+)$ is lower by about 1 eV compared to the H_2 and D_2 systems. Also, the HD system exhibits a significant intramolecular isotope effect in which $\sigma(DO_2^+)$ exceeds $\sigma(HO_2^+)$ by a factor of $\geqslant 5$. Results attributed to reaction of $O_2^+(a\,^4\Pi_u) + HD$ and D_2 are also presented, and differ appreciably from those for ground-state reactants.

Molecular orbital correlation arguments of Mahan[8] were extended to explain the observed behavior. These can reconcile the presence of a tight transition state in the entrance channel, and also show that the inefficiency of O^+ formation is due to spin conservation. Statistical phase space theory calculations are found to reproduce the branching ratios of the three major products. This agreement implies that these reactions proceed via a long-lived intermediate, consistent with the crossed beam experiments of Mahan and co-workers[6] and results of Ding, Henglein, and Bosse.[7] Quantitative comparison between theory and experiment suggests that OH^+ (OD^+) formation is restricted by about a factor of 2 relative to HO_2^+ (DO_2^+) and H_2O^+ (D_2O^+, HDO^+) formation. Phase space calculations do find that $DO_2^+ + H$ formation is favored over $HO_2^+ + D$ formation in the HD system, in agreement with the experimentally observed intramolecular isotope effect, however, the degree of enhancement is not accurately predicted. This result suggests that this effect is not solely statistical but also has additional dynamic contributions.

Finally, we have applied the translationally driven reaction theory of Marcus[18] and Chesnavich and Bowers[17] to this system. This theory is found to accurately reproduce the branching ratios between the major products, and the energy dependence and absolute magnitudes of these product cross sections. These theoretical results also show that reformation of the reactants from the intermediate complex is quite inefficient, in agreement with experimental results of Foner and Hudson.[9] The level of agreement between experiment and theory suggests that this theory should be quite useful for accurate predictions of absolute cross sections and energy dependences of additional reaction systems.

ACKNOWLEDGMENTS

This work is supported by the National Science Foundation, Grant No. CHE-9221241. P.B.A. also thanks P. A. M. van Koppen for useful conversations regarding phase space theory.

[1] K. M. Refaey and W. A. Chupka, J. Chem. Phys. **43**, 2544 (1965).
[2] J. M. Ajello, W. T. Huntress, A. L. Lane, P. R. LeBreton, and A. D. Williamson, J. Chem. Phys. **60**, 1211 (1974).
[3] W. Lindinger, D. L. Albritton, M. McFarland, F. C. Fehsenfeld, A. L. Schmeltekopf, and E. E. Ferguson, J. Chem. Phys. **62**, 4101 (1975).
[4] J. Glosik, A. B. Rakshit, N. D. Twiddy, N. G. Adams, and D. Smith, J. Phys. B **11**, 3365 (1978).
[5] K. Tanaka, T. Kato, P. M. Guyon, and I. Koyano, J. Chem. Phys. **77**, 4442 (1982); **79**, 4302 (1983).
[6] M. H. Chiang, E. A. Gislason, B. H. Mahan, C. W. Tsao, and A. S. Werner, J. Phys. Chem. **75**, 1426 (1971); E. A. Gislason, B. H. Mahan, C. W. Tsao, and A. S. Werner, J. Chem. Phys. **50**, 5418 (1969); M. H. Chiang, B. H. Mahan, C. W. Tsao, and A. S. Werner, *ibid.* **53**, 3752 (1970).
[7] A. Ding and A. Henglein, Ber. Busnsenges. Phys. Chem. **73**, 562 (1969); G. Bosse, A. Ding, and A. Henglein, *ibid.* **75**, 413 (1971).
[8] B. H. Mahan, J. Chem. Phys. **55**, 1436 (1971).
[9] S. N. Foner and R. L. Hudson, J. Chem. Phys. **36**, 2676 (1962).
[10] Revised programs are now available from the Quantum Chemistry Program Exchange, Indiana University, program No. 557. Contributors to the original and revised programs include M. T. Bowers, M. F. Jarrold, W. J. Chesnavich, L. Bass, M. E. Grice, K. Song, and D. A. Webb.
[11] M. E. Weber, J. L. Elkind, and P. B. Armentrout, J. Chem. Phys. **84**, 1521 (1986).
[12] J. L. Elkind and P. B. Armentrout, J. Phys. Chem. **89**, 5626 (1985); **90**, 5736 (1986); **90**, 6576 (1986); J. Chem. Phys. **84**, 4862 (1986); **86**, 1868 (1987).
[13] K. M. Ervin and P. B. Armentrout, J. Chem. Phys. **86**, 2659 (1987).
[14] K. M. Ervin and P. B. Armentrout, J. Chem. Phys. **84**, 6750 (1986).
[15] J. D. Burley, K. M. Ervin, and P. B. Armentrout, Int. J. Mass Spectrom. Ion Process. **80**, 153 (1987).
[16] M. E. Grice, K. Song, and W. J. Chesnavich, J. Phys. Chem. **90**, 3503 (1986).
[17] W. J. Chesnavich and M. T. Bowers, J. Phys. Chem. **83**, 900 (1979).
[18] R. A. Marcus, J. Chem. Phys. **62**, 1372 (1975).
[19] S. A. Safron, N. D. Weinstein, D. R. Herschbach, and J. C. Tully, Chem. Phys. Lett. **12**, 564 (1972).
[20] K. M. Ervin and P. B. Armentrout, J. Chem. Phys. **83**, 166 (1985).
[21] M. W. Chase, Jr., C. A. Davies, J. R. Downey, Jr., D. J. Frurip, R. A. McDonald, and A. N. Syverud, J. Phys. Chem. Ref. Data **14**, Suppl. 1 (1985).
[22] K. M. Ervin and P. B. Armentrout, J. Chem. Phys. **84**, 6738 (1986).
[23] R. H. Schultz and P. B. Armentrout, Int. J. Mass Spectrom. Ion Process. **107**, 29 (1991).
[24] S. G. Lias, J. E. Bartmess, J. F. Liebman, J. L. Holmes, R. D. Levin, and W. G. Mallard, J. Phys. Chem. Ref. Data **17**, Suppl. 1 (1988).
[25] E. R. Fisher and P. B. Armentrout, J. Chem. Phys. **94**, 1150 (1991).
[26] I. Wendel, R. A. Friedel, and M. Orchin, J. Am. Chem. Soc. **71**, 1140 (1949).
[27] K. M. Ervin and P. B. Armentrout, J. Chem. Phys. **86**, 6240 (1987).
[28] P. B. Armentrout, in *Advances in Gas Phase Ion Chemistry*, edited by N. G. Adams and L. M. Babcock (JAI, Greenwich, 1992), Vol. 1, p. 83.
[29] M. Jeunehomme, J. Chem. Phys. **44**, 4253 (1966).
[30] A. R. Fairbain, J. Chem. Phys. **60**, 521 (1974).
[31] G. Gioumousis and D. P. Stevenson J. Chem. Phys. **29**, 292 (1958).
[32] J. D. Burley, K. M. Ervin, and P. B. Armentrout, Int. J. Mass Spectrom. Ion Process. **80**, 153 (1987). The Appendix in this paper derives a critical energy of $E=(E-\Delta H)\alpha'\mu'^2/\alpha\mu^2$, where α is the polarizabil-

ity, μ is the reduced mass, ΔH is the endothermicity of reaction, and the primes refer to product channels.

[33] Energy levels for OH species were given in an MO diagram for the reaction of $OH^+ + H_2$.

[34] G. Herzberg, *Molecular Spectra and Molecular Structure. III. Electronic Spectra and Electronic Structure of Polyatomic Molecules* (Van Nostrand Reinhold, New York, 1966).

[35] The validity of this assumption has been demonstrated in W. J. Chesnavich and M. T. Bowers, J. Chem. Phys. **87**, 350 (1987).

[36] Estimates of the anharmonicities in H_2O^+, D_2O^+, and HDO^+ were obtained by scaling those of the neutrals [W. S. Benedict, N. Gailar, and E. K. Plyler, J. Chem. Phys. **24**, 1139 (1956)]. Each was reduced slightly by using the Morse potential and $D(HO^+–H)$. Also, anharmonicities for HO_2^+ and DO_2^+ are calculated in Ref. 38. Here, too, each was decreased slightly by using the Morse potential with either $D(OH^+–O)$ or $D(O_2^+–H)$.

[37] K. P. Huber and G. Herzberg, *Molecular Spectra and Molecular Structure. IV. Constants of Diatomic Molecules* (Van Nostrand Reinhold, New York, 1979).

[38] G. P. Raine, H. F. Schaefer III, and N. C. Handy, J. Chem. Phys. **80**, 319 (1984).

[39] J. M. Dyke, N. B. H. Jonathan, A. Morris, and M. J. Winter, Mol. Phys. **44**, 1059 (1981).

[40] R. Botter and J. Carlier, J. Electron Spectrosc. Relat. Phenom. **12**, 55 (1977).

[41] E. Herbst and S. K. Knudson, Chem. Phys. **55**, 293 (1981).

[42] P. J. Robinson and K. A. Holbrook, *Unimolecular Reactions* (Wiley, London, 1972).

[43] P. A. Giguère and I. D. Liu, J. Am. Chem. Soc. **77**, 6477 (1955).